JOURNAL OF MATERIALS SCIENCE 28 (1993) 5569–5575

Microwave characteristics and far-infrared reflection spectra of zirconium tin titanate dielectrics

R. KUDESIA, A. E. McHALE*, R. A. CONDRATE, Sr, R. L. SNYDER
New York State College of Ceramics, Alfred University, Alfred, NY 14802, USA

The lattice vibrations of zirconium titanate containing SnO_2 in solid solution were investigated using Fourier transform–infrared spectrophotometry. Microwave dielectric functions were determined by the Kramers–Kronig analysis followed by the classical dispersion analysis of infrared reflection spectra. The relative tendency of the spectroscopically determined dielectric functions is in agreement with those directly measured. For comparative studies or for the development of new microwave ceramic materials, the method is promising.

1. Introduction

Zirconium titanate-based dielectric ceramics show very interesting properties at microwave frequencies. These ceramics have low dielectric loss and a unique composition dependence of the temperature coefficient [1, 2]. Solid solution compositions in the ZrO_2–TiO_2–SnO_2 system are commonly used as resonator material in microwave devices [3].

Resonance methods for microwave dielectric characterization are the industry standard. They are suitable for production settings as they require significant investment in specialized equipment and a standardized sample geometry [4]. On the other hand, the relatively new infrared reflectance method is highly suitable as a research technique [5]. The reflectance method involves the determination of dielectric functions from the fundamental properties, making it quite useful for exploratory measurements on materials. No special sample geometry or sample preparation is required as is the case with resonance methods. Dielectric functions can be determined at various frequencies using only one set of data. Also, theoretically there is no high-frequency limit. The Fourier transform–infrared (FT–IR) spectrophotometer, being a versatile research instrument for materials spectroscopic investigation, is readily available in university settings, making the reflectance method a preferred technique for comparitive studies or for the development of new microwave dielectric materials. The infrared reflectance spectra may be analysed in two ways; by the Kramers–Kronig (K–K) relation or by a combined method of Kramers–Kronig integration and classical dispersion theory. The analysis by the K–K relation yields dielectric functions whose accuracy is questionable. Owing to the inherent nature of the K–K relation which requires data from zero to infinite frequency, the accuracy of the analysis is affected in trying to overcome the limitations of practical data collection. The combination of K–K relation and classical dispersion theory provides a better and more reliable procedure. Wakino *et al.* [5, 6] have calculated the dielectric constant and quality factor for TiO_2 and $Ba(Zn, Ta)O_3$–$BaZrO_3$ from the dispersion parameters which are in agreement with the measured values.

The dielectric resonator materials based on zirconium titanate solid solution with SnO_2 have a structure which is that of a high-temperature phase of pure $ZrTiO_4$ [1, 7]. The crystal structure of the high-temperature phase $ZrTiO_4$ is orthorhombic and isomorphous with α-PbO_2 (orthorhombic space group $D_{14}^{2h} = Pbcn$) [8]. The unit cell consists of two formula units. This space group implies a random distribution of the cations in available octahedral cation sites. Neutron diffraction studies have shown that the coordination octahedra of the Zr^{4+} ions are highly distorted [9].

In this study, infrared reflectivity spectra have been obtained on $Zr_xTi_ySn_zO_4$ ($x + y + z = 2$) ceramics prepared in pure form and with ZnO/La_2O_3 additives. The reflection spectra were analysed through the combination of K–K integration and classical dispersion theory. According to the classical dispersion theory, a crystal is approximated as a system of damped oscillators having an appropriate frequency and dipole moment. The real and imaginary parts of the complex dielectric constant (ε', ε'') as functions of frequency ($\nu = \omega/2\pi$) are given by the equations

$$\varepsilon'(\nu) = \varepsilon_\infty + \sum_j 4\pi\rho_j\nu_j^2 \frac{\nu_j^2 - \nu^2}{(\nu_j^2 - \nu^2)^2 + \gamma_j^2\nu^2} \quad (1)$$

and

$$\varepsilon''(\nu) = \sum_j 4\pi\rho_j\nu_j^2 \frac{\gamma_j\nu}{(\nu_j^2 - \nu^2)^2 + \gamma_j^2\nu^2} \quad (2)$$

* *Present address*: McHale Consulting, 1532 Moland Road, Alfred Station, NY 14803, USA.

0022–2461 © *1993 Chapman & Hall*

where the summation is over the j resonances in the spectrum [10]. Each resonance is characterized by its dispersion parameters which are the strength $4\pi\rho_j$, width γ_j, and frequency ν_j. The ε_∞ is the dielectric constant caused by the electronic polarization at higher frequencies.

Actual analysis involves two distinct types of calculation; Kramers–Kronig (K–K) integration and spectroscopic simulation. Kramers–Kronig analysis [10] provides approximate dispersion parameters. Starting with approximate parameters, a trial and adjustment process is used to simulate the experimental reflection spectrum.

The K–K relation used in the evaluation of the reflectivity, R, may be written as

$$\theta(\nu_m) = \frac{2\nu_m}{\pi}\int_0^\infty \frac{\ln r(\nu)}{\nu^2 - \nu_m^2}\,d\nu \quad (3)$$

where the reflectivity amplitude is $re^{i\theta}$ with $r = R^{0.5}$ and $\theta(\nu_m)$ is phase angle at a specific frequency ν_m [10]. ε' and ε'' can be obtained from

$$\varepsilon' = n^2 - k^2 \quad (4)$$

$$\varepsilon'' = 2nk \quad (5)$$

$$re^{i\theta} = [(n-1) - ik]/[(n+1) - ik] \quad (6)$$

where n is the index of refraction and k is the extinction coefficient. The K–K integral is a fundamental relationship and does not depend on any material constants. Evaluation of the K–K integral gives the approximate values of ε' and ε'' [11]. The accuracy of ε' and ε'' depends on many factors, which will be discussed in a later section. Approximate dispersion parameters are then determined from ε'' versus frequency curve, which are used to initiate the spectroscopic simulation.

2. Experimental procedure

2.1. Sample preparation

Fig. 1 shows the composition of samples prepared with no additives and the single-phase region found in an earlier study [12], which agrees with the work of Wolfram and Göbel [1]. All specimens with no additives were sintered at 1350° C for 24 h. The basic composition of the samples with ZnO/La_2O_3 ($ZnO:La_2O_3 = 1:2$) additives is $Zr_{0.8}Sn_{0.2}Ti_{1.0}O_4$. These samples were sintered at 1350° C for 16 h. After sintering, the samples were allowed to cool with the furnace. Specimens used as test objects were in round pellet shape. The pellets were polished with 600 grit (~ 17 μm) before collecting the spectra. The X-ray analysis was performed for phase identification.

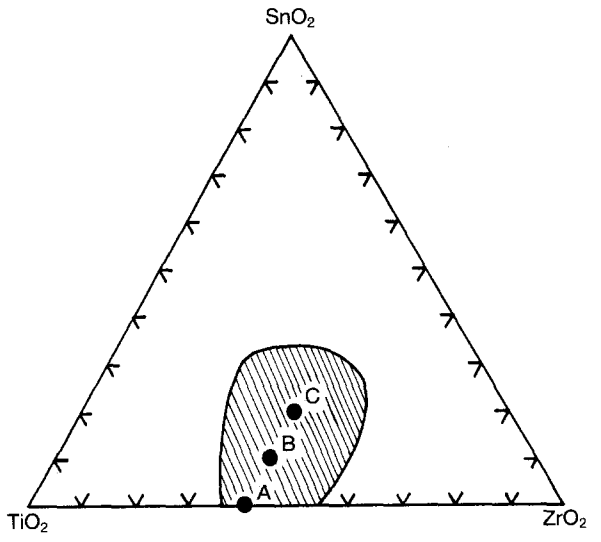

Figure 1 Composition of samples (with no additives) studied and solid solution region.

2.2. Experimental measurement technique

Nicolet 60 SXR and 20F FT–IR spectrometers with a Spectra-Tech Diffuse Reflectance accessory (DRIFT) were used to obtain the mid- and far-infrared reflection spectra, respectively. A pure gas air drier purging device attached to the instrument maintained a moisture- and CO_2-free atmosphere. The polished ceramic sample was set in the sample cup of the DRIFT accessory. The spectra were recorded over the 5000–50 cm^{-1} region. Each spectrum was scanned 320 times with a resolution of 4 cm^{-1}. The reflectivity of the sample was obtained as the intensity relative to the reflectance from a deposited aluminium mirror.

The dielectric properties of samples were directly measured at the Trans-Tech Inc. These measurements were performed at 4.2 GHz using conventional resonance techniques.

3. Analysis of data

From the reflected intensity, R, and the phase angle, $\theta(\nu_m)$ (or θ_m), the optical parameters, n and k, may be determined using the following relationships

$$n = (1 - R)/(1 + R - 2R^{0.5}\cos\theta_m) \quad (7)$$

$$k = (-2R^{0.5}\sin\theta_m)/(1 + R - 2R^{0.5}\cos\theta_m) \quad (8)$$

and hence the real and imaginary parts of dielectric constant. Because the phase angle is not experimentally determined it is generated from the reflected intensity measurements using the following K–K relationship

$$\theta_m = \frac{2\nu_m}{\pi}\int_0^\infty \frac{\ln R^{0.5}(\nu) - \ln R^{0.5}(\nu_m)}{\nu^2 - \nu_m^2}\,d\nu \quad (9)$$

The above equation has the advantages of finite integrand and minimum distortion of phase angle θ_m over Equation 3.

The K–K integral is evaluated using Maclaurin's formula. In Maclaurin's formula, every other data point is taken for the summation to avoid the difficulty around the pole part of the integration ($\nu = \nu_m$). It has been shown that this formula gives more accurate results compared to other similar numerical integration methods, and also that its computation time is short [13]. The range of integration of Equation 9 is divided into three sections: a low-frequency section, up to $\nu = \nu_l$, where $R(\nu)$ is approximately constant, the middle section of the range, and the upper section

starting from $\nu = \nu_h$, where $R(\nu)$ is again approximately constant up to high frequencies. The value of θ_m is then given by

$$\theta_m = L + H + \frac{2\nu_m}{\pi}\int_{\nu_l}^{\nu_h} \frac{\ln R^{0.5}(\nu) - \ln R^{0.5}(\nu_m)}{\nu^2 - \nu_m^2} d\nu \quad (10)$$

where

$$L = \frac{1}{2\pi}\ln\left(\frac{R_l}{R_m}\right)\ln\left|\frac{\nu_m - \nu_l}{\nu_m + \nu_l}\right| \quad (11)$$

and

$$H = -\frac{1}{2\pi}\ln\left(\frac{R_h}{R_m}\right)\ln\left|\frac{\nu_h - \nu_m}{\nu_h + \nu_m}\right| \quad (12)$$

The above relations are valid only for $\nu_l < \nu_m < \nu_h$.

The accuracy of real and imaginary parts of dielectric constant, thus obtained, depends on many factors. As the K–K expression indicates, the phase angle, θ_m, at a given frequency depends upon the reflectance amplitude $r(\nu)$ at all frequencies from zero to infinity. It is impossible to obtain data from zero to infinite frequency. The problem of limited available reflectance data has usually been approached by some sort of extrapolation procedure. Extrapolation below the lower frequency limit, ν_l, is critical to the analysis and influences the final outcome. The effect of adding extrapolations to reflectance data on the accuracy of the analysis is discussed by several workers in the literature [14, 15]. The accuracy is also dependent upon the selection of upper and lower limits for integration [15, 16]. Accuracy tends to be rather poor on the long wavelength side of the spectrum, especially in regions of low $k < 0.1$ [11].

However, each peak in the plot of ε'' versus frequency obtained from the K–K analysis represents a resonance. From the detailed characteristics of these peaks, dispersion parameters ν_j, γ_j, and $4\pi\rho_j$ are calculated for each resonance and then dielectric functions. In the approximation $\gamma_j/\nu_j \ll 1$, the frequency of a given resonance, ν_j, is the frequency at which ε_j'' is a maximum. Also, γ_j is given by the frequency half-width of the ε_j'' peak. The strength of the resonance is determined from the following relation

$$4\pi\rho_j = \gamma_j\varepsilon_j''/\nu_j \quad (13)$$

A trial and adjustment process is performed to simulate the reflectivity data with the classical dispersion theory, starting with dispersion parameters obtained from the K–K analysis. The simulation process essentially involves the following steps: (i) leaving ν_j and γ_j fixed, adjustment of ρ_j to give the correct width to the reflection band; (ii) leaving ν_j and the new ρ_j fixed, adjustment of γ_j to give the correct maximum reflectivity; (iii) finally, ν_j is adjusted to align the simulated curve with the experimental curve. Once the best fit is obtained, the loss tangent (and quality factor) can be estimated as follows under the condition of $\nu^2 \ll \nu_j^2$:

$$\tan\delta = \varepsilon''/\varepsilon' = \frac{\sum_j 4\pi\rho_j(\gamma_j\nu)/\nu_j^2}{\varepsilon_\infty + \sum_j 4\pi\rho_j} \quad (14)$$

4. Results and discussion

A factor group correlation was conducted by Krebs and Condrate for the high-temperature $ZrTiO_4$ phase [17]. The analysis, which was with the assumption of random distribution of cations, predicted the following for the optically-active first order modes of this crystal structure

$$4A_g + 5B_{1g} + 4B_{2g} + 5B_{3g} + 4A_u + 4B_{1u} + 3B_{2u} + 4B_{3u}$$

As B_{1u}, B_{2u} and B_{3u} are infrared-active, the above representation predicts eleven infrared-active modes. With the assumption that the structure of $Zr_xTi_ySn_zO_4$ $(x + y + z = 2)$ compositions is similar to that of $ZrTiO_4$, we should also expect eleven infrared-active modes. The assumption is supported by a recent neutron diffraction study on $Zr_{0.8}Sn_{0.2}Ti_{1.0}O_4$ [7].

Figs 2–5 show reflectance spectra obtained on $Zr_xSn_yTi_zO_4$ $(x + y + z = 2)$ ceramics. The infrared spectra show very broad bands. Compositions A, B and C are single-phase as was confirmed by the X-ray powder diffraction analysis of the samples. The single-phase nature of samples is in agreement with earlier studies. These samples are not expected to show any bands corresponding to the end member oxides or their solid solutions. There was no evidence of these oxide bands in any of the compositions studied, though the commercial specimen falls outside the single-phase region. The X-ray diffraction (XRD) analysis of the commercial specimen showed a SnO_2–TiO_2 solid solution phase present (see Fig. 6).

As the broadness in bands is not caused by the end-member oxide bands, other reasons were postulated. One

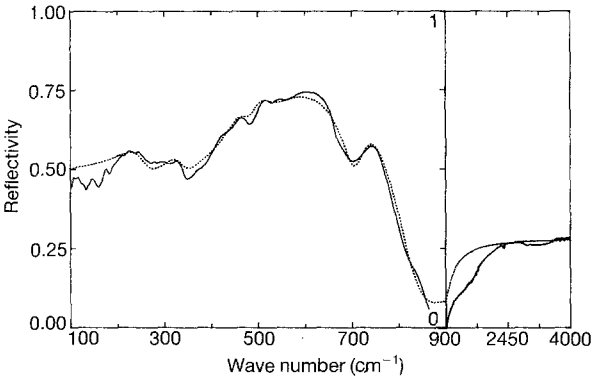

Figure 2 Infrared reflectivity of $Zr_{0.8}Sn_{0.0}Ti_{1.2}O_4$ (specimen A). (——) Observed, (. . .) simulated.

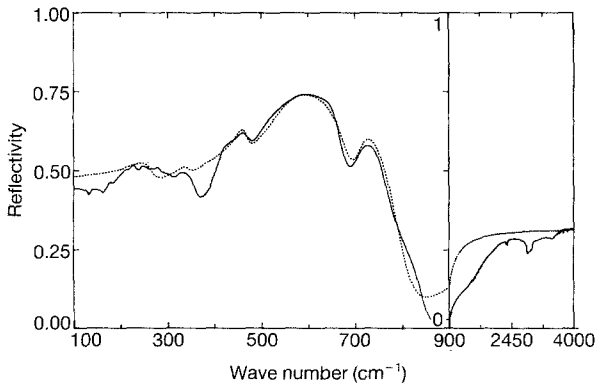

Figure 3 Infrared reflectivity of $Zr_{0.8}Sn_{0.2}Ti_{1.0}O_4$ (specimen B). (——) Observed, (. . .) simulated.

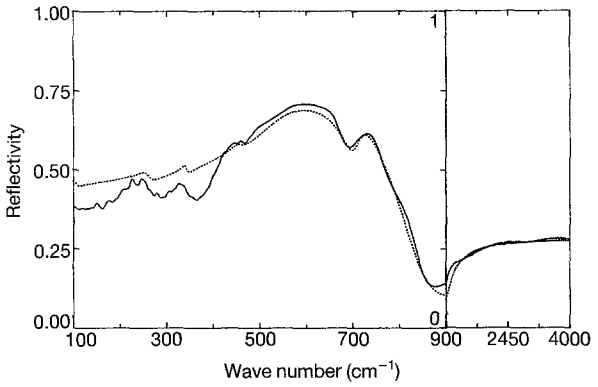

Figure 4 Infrared reflectivity of $Zr_{0.8}Sn_{0.4}Ti_{0.8}O_4$ (specimen C). (——) Observed, (. . .) simulated.

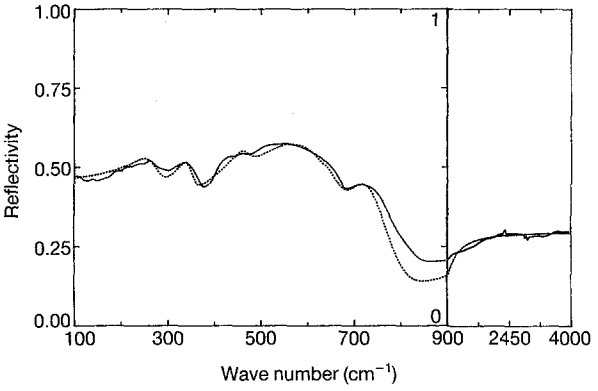

Figure 5 Infrared reflectivity of $Zr_{0.6}Sn_{0.4}Ti_{1.0}O_4$ (commercial specimen). (——) Observed, (. . .) simulated.

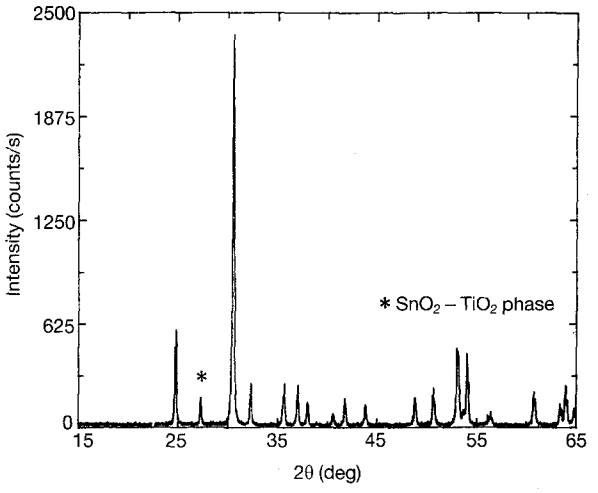

Figure 6 X-ray powder diffraction pattern of $Zr_{0.6}Sn_{0.4}Ti_{1.0}O_4$ (commercial specimen) showing SnO_2–TiO_2 as a second phase.

possible reason may be the distortion of the perfect α-PbO_2 type lattice which could also lead to apparent disorder-type effects. Krebs in his study had postulated the non-stoichiometry to cause broad bands. This, however, does not seem applicable to the zirconium tin titanate system as no significant variation from stoichiometry has been reported in the literature. From Figs 2–5, it is clear that no appreciable changes in band widths occur as titanium is replaced by tin. According to Krebs, the observed broadness in titanium-rich compounds is due to the disruption of the translational symmetry of the crystal brought about by the reduction of the oxidation state of some titanium atoms. If this is so, then one should observe the bands to broaden appreciably with increasing tin content. The probability of the reduction of Sn^{4+} to Sn^{2+} is higher than titanium reduction as the two oxidation states of tin differ little in energy. Perhaps, the increasing tin content counter-balances the effect of decreasing titanium content resulting in very small or no change in band widths for the studied compositions.

The spectra for these ceramic materials consist mainly of a strong broad band at around 550 cm^{-1}, one weak shoulder at about 700 cm^{-1} and three medium to weak bands below 550 cm^{-1}. These results are in agreement with earlier work by Krebs on $ZrTiO_4$ [17]. He also observed only five bands in the infrared spectrum. No bands are observed above 800 cm^{-1} and below 100 cm^{-1}. Bands may not be observed due to either the low band intensities or band overlap between a pair of bands. It is also possible that bands might appear below 100 cm^{-1}. As the noise level in this frequency region is quite high, no definite conclusions are possible. For K–K analysis, the far-infrared reflectance data below 80 cm^{-1} were not taken into account for the above-mentioned reason. Instead, each spectrum was extrapolated from the available reflectance trend just above 80 cm^{-1}.

Fig. 7 is a typical plot of ε″ versus frequency obtained after the K–K analysis of data. The starting parameters for classical dispersion analysis were determined from various peaks in the ε″ versus frequency plot. Starting with these parameters, the reflectivity curve was simulated. In the case of two or three resonant modes, the spectroscopic simulation procedure, described in the earlier section, works very well. However, if a large number of resonant modes are present, then the procedure requires repeated steps of trial and adjustment, especially when some of the modes overlap with each other. When there is overlapping of bands, the starting parameters cannot be determined accurately as the peaks are not clearly resolved in ε″ versus frequency curve. After trial and adjustment, the best simulated curve was obtained. Figs 2–5 also include simulated reflectance curves. The final dispersion parameters corresponding to the best

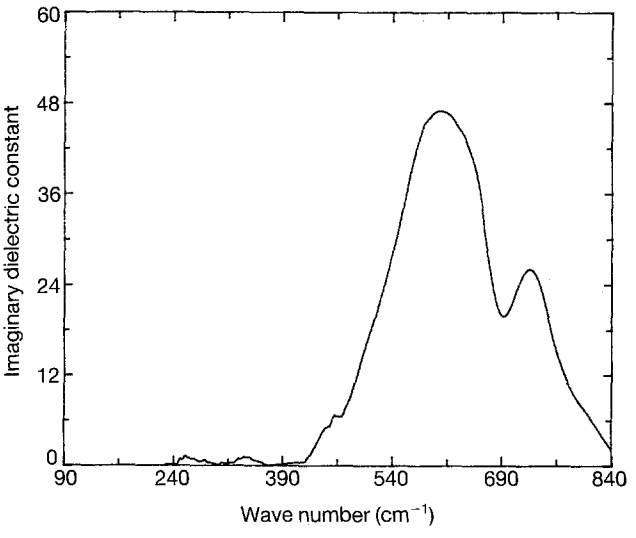

Figure 7 ε″ versus frequency for $Zr_{0.8}Sn_{0.4}Ti_{0.8}O_4$ (specimen C). Each peak represents a resonance.

TABLE I Dispersion parameters obtained by trial and adjustment process to the reflectivity data for zirconium titanate samples

Specimen A $Zr_{0.8}Sn_{0.0}Ti_{1.2}O_4$			Specimen B $Zr_{0.8}Sn_{0.2}Ti_{1.0}O_4$			Specimen C $Zr_{0.8}Sn_{0.4}Ti_{0.8}O_4$			Commercial specimen $Zr_{0.6}Sn_{0.4}Ti_{1.0}O_4$		
ν_j (cm^{-1})	γ_j (cm^{-1})	$4\pi\rho_j$	ν_j (cm^{-1})	γ_j (cm^{-1})	$4\pi\rho_j$	ν_j (cm^{-1})	γ_j (cm^{-1})	$4\pi\rho_j$	ν_j (cm^{-1})	γ_j (cm^{-1})	$4\pi\rho_j$
						105	20	0.45			
245	70	4.83	260	50	2.21	260	15	0.23	265	60	3.56
330	50	1.65	343	25	0.34	343	20	0.17	343	35	1.44
460	50	3.78	462	27	1.67	455	35	0.72	462	45	1.17
500	50	3.60									
530	180	3.20									
550	110	3.64	550	95	12.23	545	132	8.08	550	168	8.93
									640	15	0.01
720	50	0.27	710	50	0.44	710	40	0.16	710	75	0.54
$\varepsilon_\infty = 10.13$			$\varepsilon_\infty = 12.82$			$\varepsilon_\infty = 6.62$			$\varepsilon_\infty = 11.56$		

TABLE II Quality factor (at 4.2 GHz) of zirconium titanate samples with no additives

Sample	Composition	Calculated Q	Measured Q	Calculated K	Measured K
A	$Zr_{0.8}Sn_{0.0}Ti_{1.2}O_4$	19 500	–	31.1	–
B	$Zr_{0.8}Sn_{0.2}Ti_{1.0}O_4$	36 000	13 000	29.7	37.6
C	$Zr_{0.8}Sn_{0.4}Ti_{0.8}O_4$	25 500	–	16.4	–
Commercial[a]	$Zr_{0.6}Sn_{0.4}Ti_{1.0}O_4$	22 200	12 000	27.2	–

[a] Nominal sample composition and measured loss characteristics were provided by Dr T. Negas of Trans Tech, Inc.

simulated curves are listed in Table I. These final dispersion parameters were used to calculate the dielectric loss at 4.2 GHz.

Reflectivity curves were simulated considering five resonant modes. However, for sample A ($Zr_{0.8}Sn_{0.0}Ti_{1.2}O_4$), five resonant modes do not completely describe the reflectivity data. The ε'' versus frequency curve for this sample indicates that two additional resonant modes at 500 and 530 cm^{-1} are present. The observed reflectivity, in this case, was simulated by including these two modes. For sample C ($Zr_{0.8}Sn_{0.4}Ti_{0.8}O_4$), an extra mode at 105 cm^{-1} was observed. For the commercial sample, another mode at 640 cm^{-1} was present. The strength of this mode, however, is very low compared to other modes. Thus, in general, for zirconium tin titanate, dispersion parameters with five resonances give a resonable fit to the observed reflectivity data.

The dielectric characteristics were calculated from the dispersion parameters listed in Table I. The resultant dielectric losses at 4.2 GHz are tabulated in Table II. For composition A with no tin, a quality factor value of 19 500 is obtained. Sample B ($Zr_{0.8}Sn_{0.2}Ti_{1.0}O_4$) shows a calculated Q-value of 36 000. The directly measured Q-value for composition B is 13 000. The higher Q-factor of sample B compared to that of sample A is consistent with the fact that zirconium tin titanate solid solution compositions are good low-loss microwave dielectrics. Tin substitution apparently stabilizes the high-temperature structure. In the case of sample A, the cooling cycle results in at least partial ordering of the structure, causing lower Q-factor. The presence of two additional bands at 500 and 530 cm^{-1} also indicates a different structural state of this sample. However, a low Q-factor (25 500) is calculated for sample C. The degradation of the Q-factor is probably caused by the overall lowering of reflectivity. The calculated and measured Q-factors of the commercial specimen are 22 200 and 12 000, respectively.

The relative tendency of calculated quality factor (i.e. inverse tan δ) values are in good agreement with the directly measured values. However, the calculated Q-factors are higher than those directly measured or expected for ceramics of these compositions. It is known that not all modes, which contribute to the dielectric loss, are infrared active. In addition, the truncation of data below 80 cm^{-1}, together with the observation of only six or seven resonances (instead of eleven as predicted by factor group analysis) may result in an underestimation of the dielectric loss and an overestimation of quality factor. Wakino, in 1986, reported that for composition $Zr_{0.7}Sn_{0.3}Ti_{1.0}O_4$ the spectra is well fit with six resonant modes [18], in agreement with the present work. No bands were observed below 100 cm^{-1} but the calculated Q was underestimated in contrast to the results obtained in this study. However, our speculation regarding the undetected resonant modes is supported by the observation that the calculated dielectric constant for these compositions are lower than directly measured or expected values. The dielectric constant for the dense ceramics of the studied compositions should be 35–42 depending on the tin content. The calculated values are underestimated but follow the right trend. The calculated value of the dielectric constant in the microwave frequency regime is proportional to the number of resonances observed. The strength of the resonant mode adds to the dielectric constant. The presence of any resonant mode, other than observed ones, will contribute to the calculated dielectric constant thus providing better agreement with the measured value, for

cases studied here. The same may be argued for the quality factor data. Therefore, the overestimation of the Q-factor with the available data due to the presence of more bands below 100 cm^{-1} is a reasonable argument.

The possibility of the additional resonant modes in the frequency region below 100 cm^{-1} deserves further discussion. Such resonant modes may be underdamped ($\gamma_j/\nu_j < 1$) or overdamped ($\gamma_j/\nu_j > 1$). Underdamped modes have positive values of $4\pi\rho_j$, and thus increase total tan δ, whereas overdamped modes reduce the sum. Thus, if undetected resonant modes below 100 cm^{-1} are responsible for the high values of calculated Q-factors, it is expected that they will be underdamped modes.

Other factors affect the quality factor value when measured using resonance techniques. Microstructural flaws are known to reduce the measured Q. However, the reflection measurement is thought to be much less sensitive to specimen morphology and perfection. The microstructure of the specimens prepared for this study was not controlled and was not expected to yield high Q-values in conventional resonance measurements. One may notice a better agreement between the calculated and measured Q-factor of commercial specimen due to presumably better microstructure. Therefore, the estimates of the quality factor given in Table II provide lower limits for the loss tangent of these ceramic compositions.

Another series of samples (base composition $Zr_{0.8}Sn_{0.2}Ti_{1.0}O_4$) with varying concentration of sintering aids, ZnO/La_2O_3, were analysed in a similar manner. Again, The reflectivity spectra were fit with five resonances. Table III gives the dispersion parameters which were used to fit the spectra. Figs 8 and 9 show observed and simulated reflectance spectra obtained on LZ60 (0.60 wt % additives) and LZ25 (2.25 wt % additives), respectively. The calculated and directly measured dielectric functions (at 4.2 GHz) are tabulated in Table IV. The results show that the quality factor degrades significantly with the addition of sintering aids. The degradation is probably the overall effect of additive's solubility in zirconium tin titanate structure and changing microstructure. The calculated quality factor values show similar trends. The overestimated Q-factors degrade with increasing amount of additives but not as adversely as the measured values. The calculated dielectric constant values are much lower, again indicating that not all resonances are seen in the spectra. Normally the dielectric constant for these compositions is around 36–37. The sample LZ25 shows a slightly higher calculated K and lower Q-factor. This somewhat significant change is caused by the relatively stronger bands at 262 and 341 cm^{-1} as compared to other samples. A higher concentration of additives, 2.25 wt %, results in stronger bands at these wave numbers, affecting the calculated dielectric functions.

TABLE III Dispersion parameters obtained by trial and adjustment process to the reflectivity data for $Zr_{0.8}Sn_{0.2}Ti_{1.0}O_4$ samples with ZnO and La_2O_3

Sample (additive wt %)	ν_j (cm^{-1})	γ_j (cm^{-1})	$4\pi\rho_j$
LZ60 (0.60 wt %)			
$\varepsilon_\infty = 9.46$	265	47	2.42
	345	35	1.09
	460	50	4.73
	530	65	8.01
	702	45	0.19
LZ50 (1.50 wt %)			
$\varepsilon_\infty = 9.70$	263	50	2.89
	343	18	0.68
	460	50	4.02
	528	75	8.88
	705	42	0.21
LZ25 (2.25 wt %)			
$\varepsilon_\infty = 10.33$	262	70	5.09
	341	30	1.29
	459	50	4.27
	528	76	8.97
	705	42	0.22

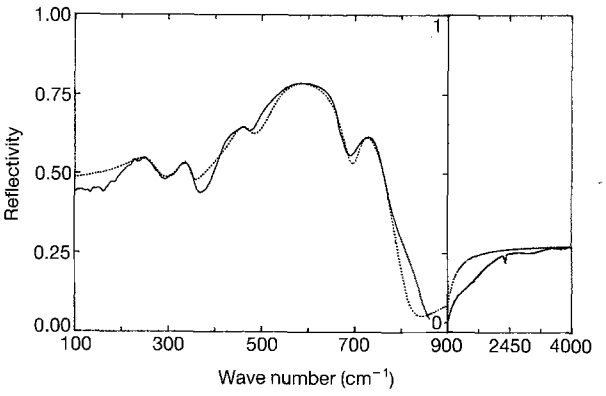

Figure 8 Infrared reflectivity of LZ60 ($Zr_{0.8}Sn_{0.2}Ti_{1.0}O_4$ with 0.60 wt % ZnO/La_2O_3). (———) Observed, (. . .) simulated.

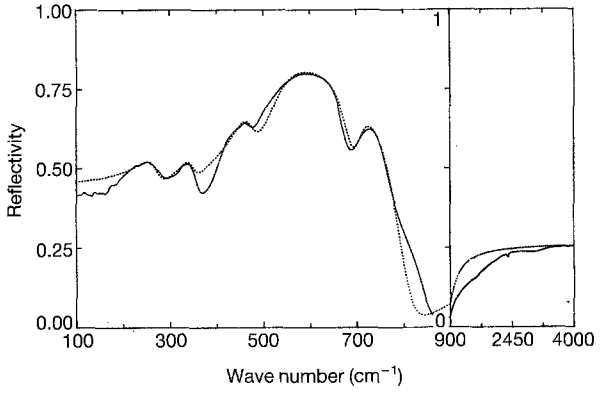

Figure 9 Infrared reflectivity of LZ25 ($Zr_{0.8}Sn_{0.2}Ti_{1.0}O_4$) with 2.25 wt % ZnO/La_2O_3). (———) Observed, (. . .) simulated.

TABLE IV Calculated and measured dielectric functions (at 4.2 GHz) of $Zr_{0.8}Sn_{0.2}Ti_{1.0}O_4$ samples with additives (ZnO/La_2O_3)

Sample	Calculated Q	Measured Q	Calculated K	Measured K
LZ60	37 000	9700	25.9	–
LZ50	34 000	5300	26.4	–
LZ25	24 500	3600	30.2	36.7

5. Conclusions

It is concluded from this study that far infrared reflectance data can be used to determine the relative trends of the dielectric functions at microwave frequencies.

The analysis of the reflectance data by combined method of Kramers–Kronig integration and classical dispersion theory is more reliable compared to only Kramers–Kronig analysis. The Kramers-Kronig analysis followed by classical dispersion analysis reduces sources of potential error and uncertainties and appears to be a more reliable method. This procedure does not require any extensive data extrapolation process, as is the case if only Kramers–Kronig analysis is used. Calculated loss tangents tend to be underestimated using this technique. However, dielectric functions can be obtained at the high gigahertz frequencies where resonance methods do not give reliable values.

This method could be used in practice to determine the critical importance of ceramic preparation and microwave material, through comparison with resonance cavity determinations of the quality factor. The dielectric functions are obtained from the fundamental material characteristics, and the sample preparation is quite flexible. Thus, this technique could be very useful in the development of new microwave ceramic dielectrics.

Acknowledgements

This research was funded by the Center of Advanced Ceramic Technology at NYS College of Ceramics, Alfred University, Alfred, NY, USA.

References

1. G. WOLFRAM and H. E. GÖBEL, *Mater. Res. Bull.* **16** (1981) 4155.
2. K. WAKINO, K. MINAI and H. TAMARA, *J. Am. Ceram. Soc.* **67** (1984) 278.
3. M. KATSUBE, Y. ISHIKAWA, H. TAMURA, and K. TOMONO, US Pat. 4102696, 25 July, 1978.
4. W. E. COURTNEY, *IEEE Trans. Microwave Theory Tech.* **18** (1970) 476.
5. K. WAKINO, D. A. SAGALA and H. TAMURA, *Jpn J. Appl. Phys.* **24** Suppl 24–2 (1985) 1042.
6. K. WAKINO and H. TAMURA, Abstract no. 24-E-87, 89th Annual Meeting of the American Ceramic Society, Pittsburgh, PA, USA, 26–30 April, 1987 (unpublished).
7. R. KUDESIA, PhD thesis, Alfred University, Alfred, USA (1992); R. KUDESIA, R. L. SNYDER, R. A. CONDRATE, Sr, and A. E. McHALE, *J. Phys. Chem. Solids* **54** (1993) 671.
8. R. E. NEWNHAM, *J. Am. Ceram. Soc.* **50** (1967) 216.
9. P. BOURDET, A. E. McHALE, A. SANTORO and R. S. ROTH, *J. Solid State Chem.* **64** (1986) 30.
10. W. G. SPITZER, R. C. MILLER, D. A. KLEINMAN and L. E. HOWARTH, *Phys. Rev.* **126** (1962) 1710.
11. W. G. SPITZER and D. A. KLEINMAN, *ibid.* **121** (1961) 1324.
12. A. H. LEE, MS thesis, Alfred University, Alfred, USA (1988).
13. K. OHTA and H. ISHIDA, *Appl. Spectrosc.* **42** (1988) 952.
14. F. STERN, "Solid State Physics", Vol. 15 (Academic Press, London, 1963) p. 337.
15. G. ANDERMANN, A. CARON, and D. A. DOWS, *J. Opt. Soc. Am.* **55** (1965) 1210.
16. R. KUDESIA and A. E. McHALE, in "Advanced Characterization Techniques for Ceramics", edited by W. S. YOUNG, G. L. McVAY, and G. E. PIKE (American Ceramic Society, Westerville, USA, 1990) p. 420.
17. M. A. KREBS, PhD thesis, Alfred University, Alfred, USA (1982); M. A. KREBS and R. A. CONDRATE, Sr, *J. Mater. Sci. Lett.* **7** (1988) 1327.
18. K. WAKINO, "Microwave Characteristics of $Zr_{0.7}Sn_{0.3}Ti_{1.0}O_4$", Dielectric Resonator Workshop, Microwave Theory and Techniques, International Symposium, Baltimore, USA, 1986 (unpublished).

Received 17 September 1992
and accepted 11 March 1993